Characteristics of the Inlet with the Pressure Perturbation in the Ramjet Engine

Dongshin Shin*, **Hochul Kang**
Department of Mechanical System Design Engineering, College of Engineering, Hongik University, Seoul 121-791, Korea

Flows in a ramjet inlet is simulated for the study of the rocket-ramjet transition. The flow is unsteady, two-dimensional axisymmetric, compressible and turbulent. Double time marching method is used for the unsteady calculation and HLLC method is used as a higher order MUSCL method. As for turbulent calculation, $k-\omega$ SST model is used for more accurate viscous calculations. Sinusoidal pressure perturbation is given at the exit and the flow fields at the inlet is studied. The cruise condition as well as the ground test condition are considered. The pressure level for the ground test condition is relatively low and the effect of the pressure perturbation at the combustion chamber is small. The normal shock at the cruise condition is very sensitive to the pressure perturbation and can be easily detached from the cowl when the exit pressure is relatively high. The sudden decrease in the mass flux is observed when the inlet flow becomes subcritical, which can make the inlet incapable. The amplitude of travelling pressure waves becomes larger as the downstream pressure increases, and the wavelength becomes shorter as Mach number increases. The phase difference of the travelling perturbed pressure wave in space is 180 degree.

Key Words : Ramjet Inlet, Rocket-Ramjet Transition, Compressible

Nomenclature

Q	: Conservation variable
E, F, G	: Convective flux
E_v, F_v, G_v	: Diffusive Flux
ξ, η, ζ	: Computational coordinates
J	: Jacobian
f	: Frequency
p	: Pressure
M	: Mach nNumber
T	: Period

1. Introduction

The ramjet inlet is designed to efficiently reduce the flow velocity relative to the engine so that the burning in the combustion chamber may remain stable. However, experiences show that the undesired phenomenon may sometimes arise in the subcritical operating condition, leading to combustion instability, engine surge, and thrust loss, which result in deterioration of the performance of the propulsion system. The characteristics involved in the ramjet inlet was studied by experiment (Dailey, 1955). The phenomenon can be categorized as one of the many self-excited flows that occur in fluid mechanics. It is generally agreed that a self-excited flow must be formed in a closed-loop manner, which consists mainly of two mutually interactive elements, namely, an origin of instability wave, and an upstream feedback mechanism. The acoustic wave often plays the role of upstream feedback because the entropy and vorticity waves are convective waves that flow downstream with the stream (Lu and Jain, 1998). For high speed inlet flow, these basic

* Corresponding Author,
E-mail : dsshin@hongik.ac.kr
TEL : +82-2-320-1477; **FAX** : +82-2-324-8911
Department of Mechanical System Design Engineering, College of Engineering, Hongik University, Seoul 121-791, Korea. (Manuscript **Received** October 7, 2005; **Revised** January 6, 2006)

elements and their interactions are not clearly understood. The present work attempts to analyze the inlet flow with the pressure perturbation in the ramjet engine numerically.

The Navier-Stokes computations concerning the unsteady inlet flow were first conducted by Newsome (1984) using the MacCormack explicit scheme. Shigematsu and Yamamoto (1990) also performed an inlet flow calculation by using a flow plug in the rear of a two-dimensional ramjet to facilitate the control of the back pressure and the mass flux. These numerical simulations indicate that analyzing the unstable inlet flow by means of numerical approach is promising.

The main objective of this work is to study the flow fields at the inlet when the pressure perturbations exist in the combustion chamber. The Mach number considered is 2.5 which is the design Mach number whereas the off-design Mach numbers 2 and 3 are also examined. The parameters considered are the velocity and the back pressure. Finally, the magnitude of perturbation at each Mach number that can affect the incoming mass flux is studied.

2. Numerical Method

The boundary-layer effects and the flow separation phenomenon are very important in the inlet flow simulations (Kim, 2004), and the Reynolds-averaged Navier-Stokes equations are adopted as the governing equations. In the finite volume approach, the volume integral of the governing equations can be written as follows.

$$\int_{\Omega}\left[\frac{\overline{\partial Q}}{\partial t}+\frac{\overline{\partial E}-\overline{\partial E_v}}{\partial \xi}+\frac{\overline{\partial F}-\overline{\partial F_v}}{\partial \eta}+\frac{\overline{\partial G}-\overline{\partial G_v}}{\zeta}\right]d\Omega=0 \quad (1)$$

Using appropriate spatial discretization, Eq. (1) can be written as follows.

$$\frac{1}{J}\frac{dQ_{ijk}}{dt}+R_{ijk}=0 \quad (2)$$

Here R_{ijk} is the residual and can be written as follows.

$$R_{ij}=E_{i+1/2,j,k}-E_{i-1/2,j,k}+F_{i,j}+_{1/2,k}+G_{i,j,k+1/2}-G_{i,j,k-1/2} \quad (3)$$

Here subscripts $i+1/2$ and $i-1/2$ represent the left and right boundary faces of each control volume. The same rule applies j and k directions. The temporal variation of a flow variable for each cell is equal to the difference of the fluxes that pass the control surfaces.

The general Flux-Difference-Splitting scheme of Roe (1981) has some difficulty of the carbuncle along the stagnation line or the expansion shock when the sharp expansion exists. The entropy correction method is used to improve the simulation, which leads to the thick shock and less accuracy in the boundary layer simulation. Recently, Harten-Lax-Leer-Contact surface method (Toro, 1997) is introduced to satisfy the entropy requirements and is used for the present study. Since the present study requires the turbulent viscous simulation, the ADI method with the double time marching is adopted for the time integration. As for turbulence model, we used the improved $k-\omega$ SST model by Menter (1994) because the $k-\omega$ turbulent model proposed by Wilcox (1988) is known to be very sensitive to the far field velocity.

For viscous boundary implementation, the wall boundary condition is applied at the walls. The characteristic exit condition (Wilcox, 1988) is adopted because the speed at the exit is subsonc. The exit pressure is given as the sinusoidal function with the frequency of 500 Hz that is the usual frequency for a ramjet combustor pressure perturbation.

$$p=p_{outlet}[1+0.2\sin(2\pi ft)] \quad (4)$$

Figure 1 shows the computational grid that has two blocks. The block that includes the inlet passage consists of 212×41 grids and the other block 94×36 grids, respectively. The grids are clustered near the wall to make the minimum $y^+\approx 1$. The physical time step is 1/100 of one period of the perturbation sinusoidal function.

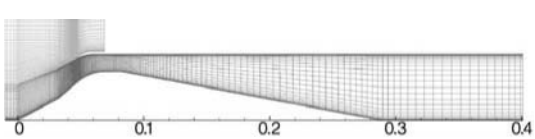

Fig. 1 Computational grid

3. Characteristics of the Inlet at the Ground Test Condition

The ground test condition considered here is at the height of 12.8 km, where the static pressure is 0.171 atm and the static temperature is 90 K. To investigate the characteristics of the inlet flow fields due to the pressure perturbation at the combustion chamber, we used the sinusoidal forcing with 20% magnitude of the exit pressure. The back pressure was controlled to locate the normal shock at the 1/3 position from the neck to the exit. First, the steady state solution is obtained for the above back pressure and the unsteady simulation is performed from the obtained steady solution as an initial state. Figure 2 shows the pressure distribution over the one period when the Mach number is 2.5 (design Mach number).

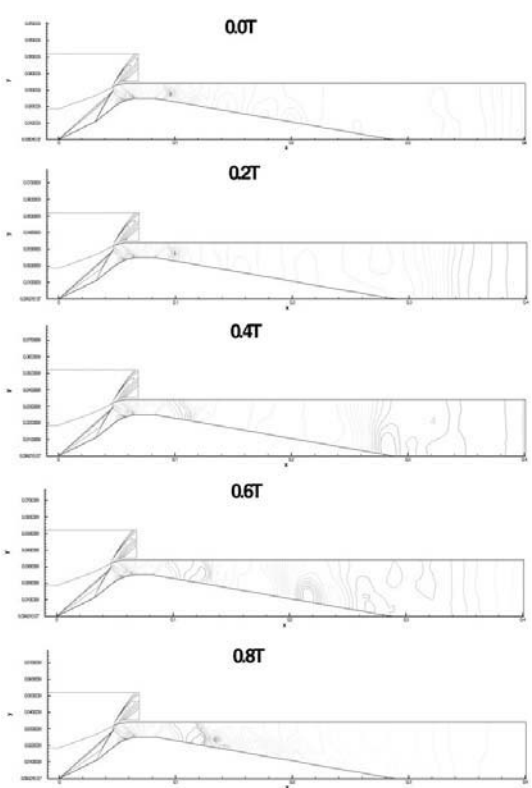

Fig. 2 Contours of pressure distribution over the one period at the ground test condition. $M=2.5$, $p_b/p_i=8$

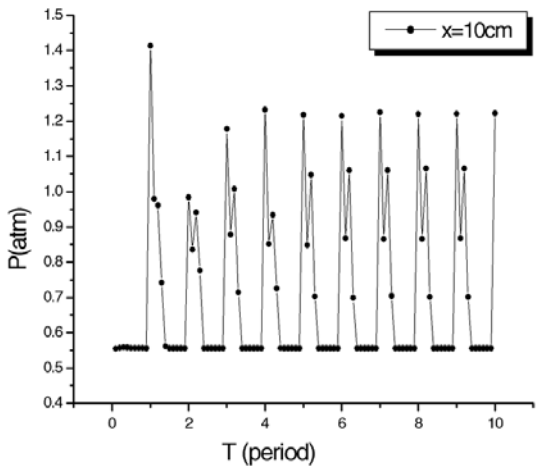

(a) $x=10$ cm

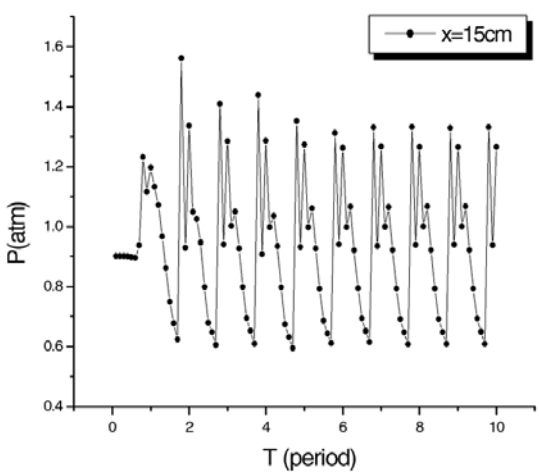

(b) $x=15$ cm

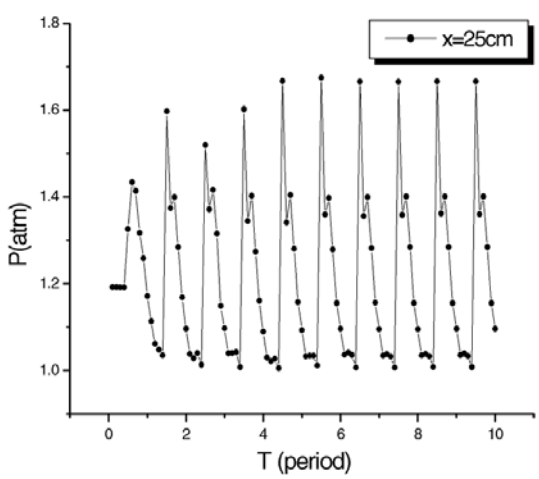

(b) $x=25$ cm

Fig. 3 Pressure response at the center line at the ground test condition. $M=2.5$, $p_b/p_i=8$

The corresponding back and inlet pressure ratio is 8. The normal shock is standing right after the neck at 0.0T. At 0.2T, the normal shock moves to the neck and becomes weak, and another pressure wave appears near the exit due to the pressure perturbation. The pressure wave near the exit starts to move to the neck over the period of 0.4T and 0.8T. Figure 3 shows the pressure responses over 10 time periods at different locations of the center body. Here the Mach number is 2.5 and the other Mach number cases show the similar behavior. They show the periodic pressure response after the third period. The pressure responses at $x=10$ cm in Fig. 3(a) show the moving of normal shock with time. Figure 4 shows the pressure difference from the steady state one along center body at different time periods. It shows that perturbed pressure wave moves from the exit to the neck of the inlet as time goes by, which moves the normal shock near the neck back and forth. The change of the normal shock location with time is small because the overall pressure level is relatively low and the magnitude of the perturbed pressure wave is almost the same as that of the forcing at the exit.

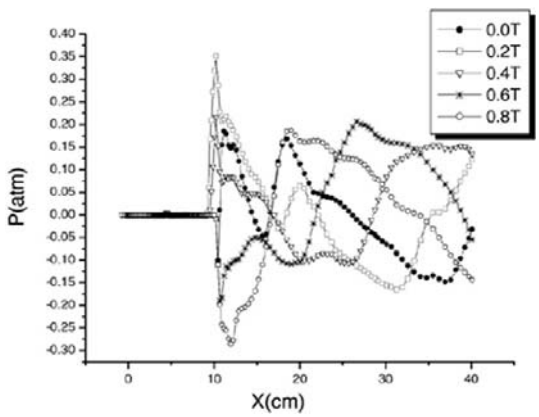

(a) $M=2$, $p_b/p_i=5$

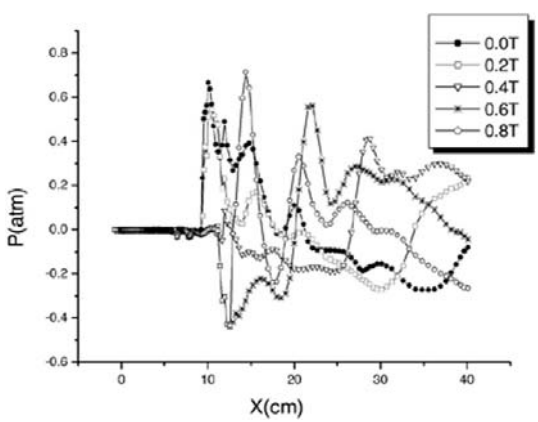

(b) $M=2.5$, $p_b/p_i=8$

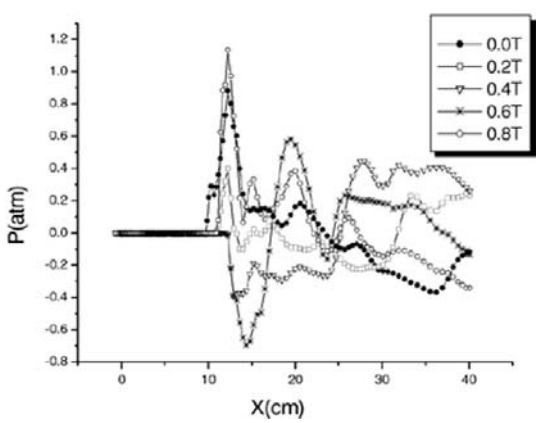

(b) $M=3$, $p_b/p_i=10$

Fig. 4 Pressure difference from the steady state one along the center body at the ground test condition

4. Characteristics of the Inlet at the Cruise Condition

The pressure level for the ground test condition is relatively low and the effect of the perturbation at the combustion chamber to the inlet flow fields is very small. To investigate the effect of the perturbation at the cruise condition, we considered the flow fields at the height of 2.5 km and the downstream pressure that is very close to the one at the real combustion chamber. The corresponding static pressure is 0.74 atm and the static temperature is 272 K. The downstream pressure range covers from 4.5 to 10 atm according to the Mach numbers.

Figures 5～7 show the pressure distribution at different Mach numbers and Figure 8 shows the pressure difference from the steady state one along center body at different time periods. Figure 5 shows the pressure distribution over the one period when the Mach number is 2. The normal shock is detached from the cowl and becomes the bow shock when the Mach number is 2 and the

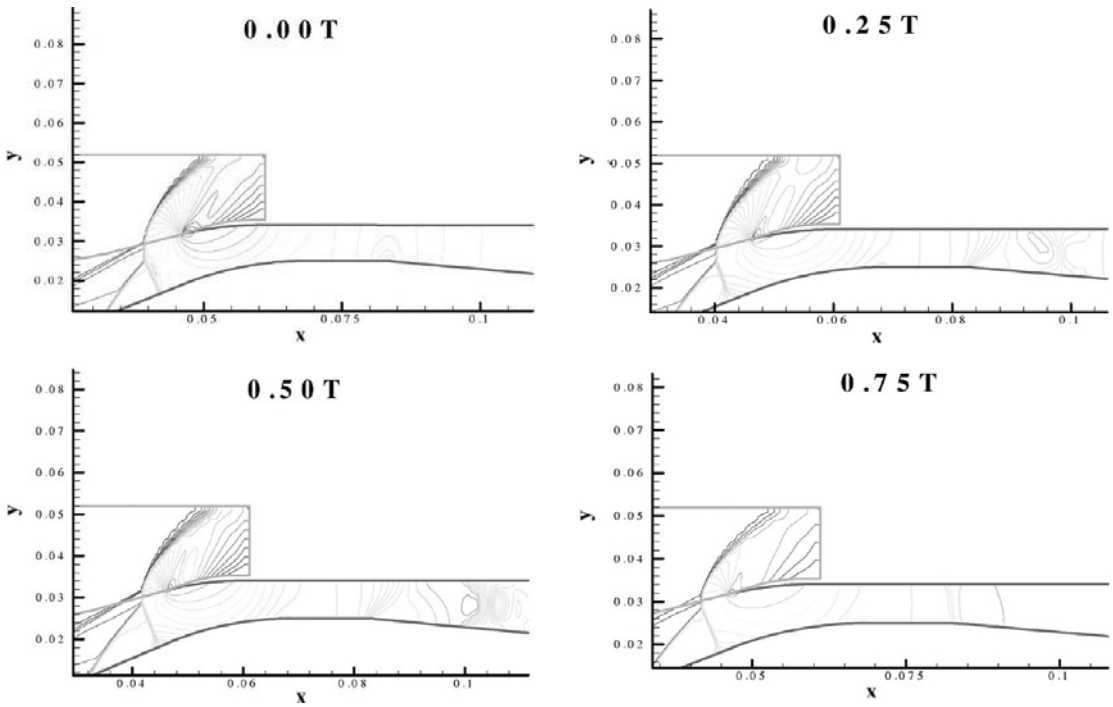

Fig. 5 Contours of pressure distribution over the one period at the cruise condition. $M=2$, $p_b=4.5$ atm, $p_b/p_i=6.081$

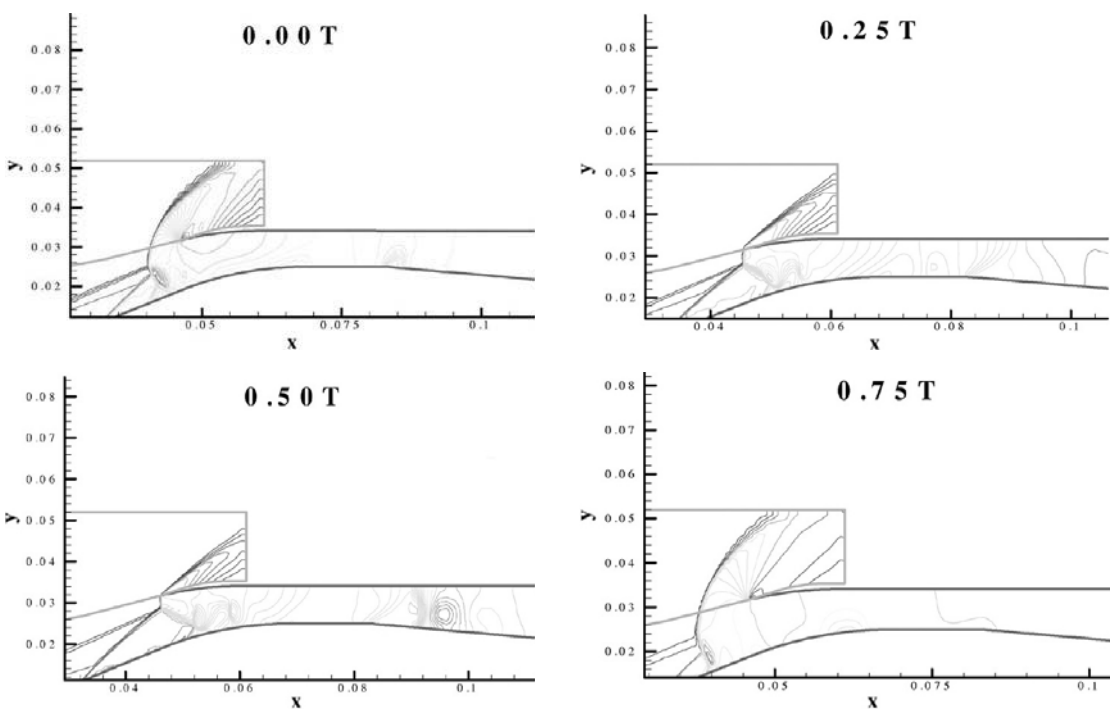

Fig. 6 Contours of pressure distribution over the one period at the cruise condition. $M=2.5$, $p_b=7.0$ atm, $p_b/p_i=9.459$

pressure ratio is 6.5. To avoid this kind of behavior, the exit pressure is set to be 4.5 atm. The rate of the perturbation magnitude is set to be 10% because 20% perturbation makes the normal shock be detached and be the bow shock in front of the cowl. The downstream perturbation becomes maximum at 0.25T and minimum at 0.75T, respectively. It shows that the normal shock at the neck and the bow shock in front of the cowl spread to backward at 0.25T but they merge and become sharp at 0.75T. When Mach number is 2.5, the design Mach number, and the exit pressure is 5 atm, the pressure distribution shows that the normal shock locates after the neck and moves back and forth with time. The pressure difference in Fig. 8(b) shows this behavior. The rate of the perturbation magnitude is set to be 20% at this Mach number. The normal shock moves upstream when the exit pressure is increased to 6 atm and the pressure distribution shows similar characteristics. The pressure difference in Fig. 8(c) shows that the wave length of the pressure wave does not change but the magnitude becomes large, and the location of the normal shock moves upward. If the exit pressure is increased to 7 atm, the normal shock reaches almost the center of the neck and becomes unstable. Figure 6 shows the pressure distribution over the period in this case. With the pressure perturbation, the normal shock passes through the neck and stays in front of the neck (0.25T) but it comes back and stays after the neck (0.5T). If the numerical method does not have enough accuracy, it is hard to catch this kind of behavior. The pressure distribution in Figure 6 shows the unsteady behavior of the shock that departs the inlet and enters into the neck with time. The pressure difference in Fig. 8(d) shows that the pressure gradient is very large outside of the cowl compared with the one inside the inlet. The perturbation at the combustion chamber can change the outside flow field at this condition. If the exit pressure is increased to 8 atm, the normal shock is completely detached from the cowl and the effect of the perturbation can not be seen. If we increase the Mach number to 3 at exit pressure 6 atm, the normal shock stays further downstream

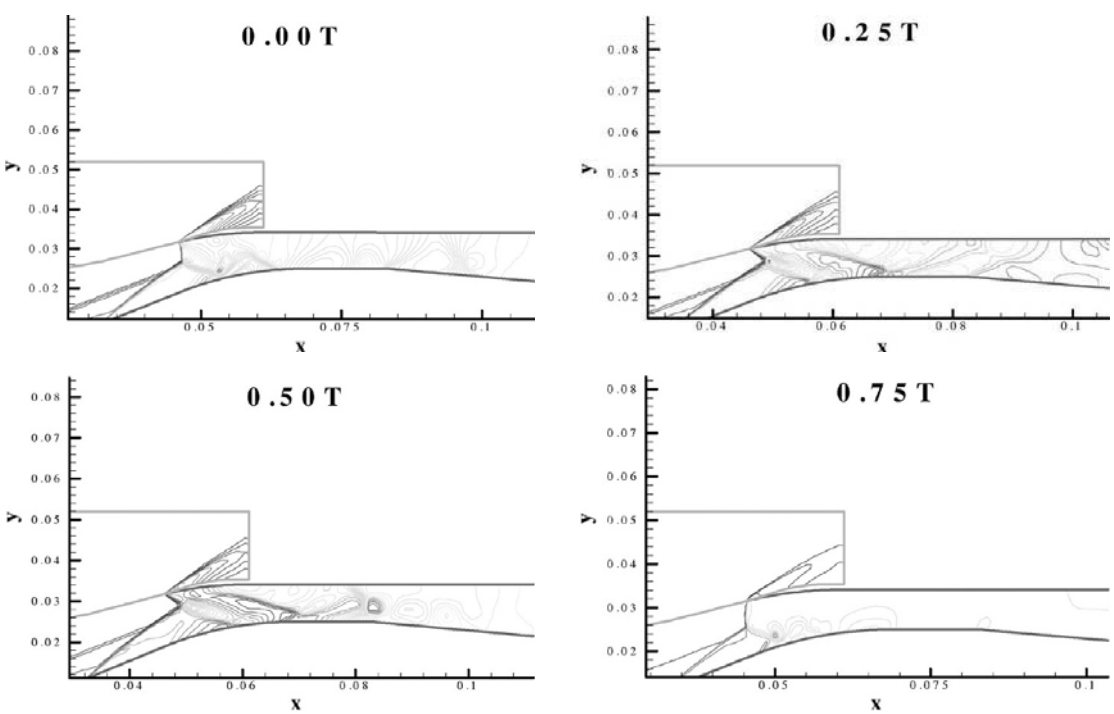

Fig. 7 Contours of pressure distribution over the one period at the cruise condition. $M=3$, $p_b=10.0$ atm, $p_b/p_i=13.513$

compared to the Mach number 2.5 case. The pressure difference in Fig. 8(e) shows that the wavelength of the pressure wave becomes shorter and it agrees well with the fact that the wavelength and the Mach number is inversely proportional. It also shows that the phase difference of the wave in space is 180 degree. When the perturbation pressure reaches maximum at the exit,

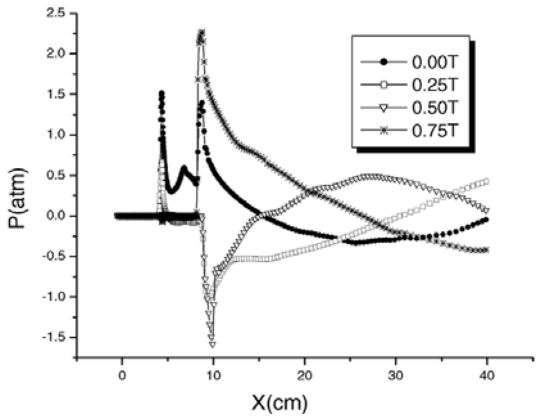

(a) $M=2$, $p_b=4.5$ atm, $p_b/p_i=6.081$

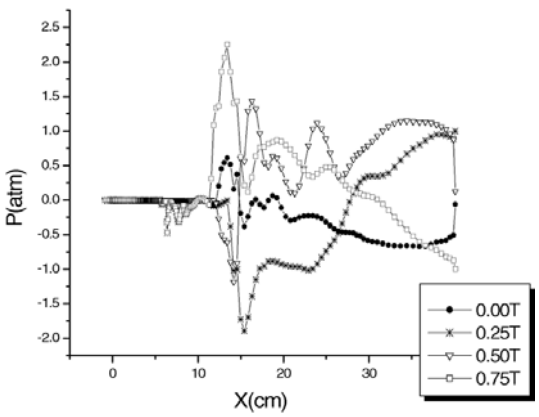

(b) $M=2.5$, $p_b=5.0$ atm, $p_b/p_i=6.7567$

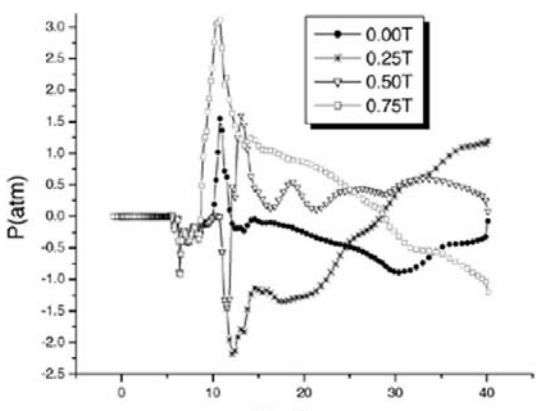

(c) $M=2.5$, $p_b=6.0$ atm, $p_b/p_i=8.108$

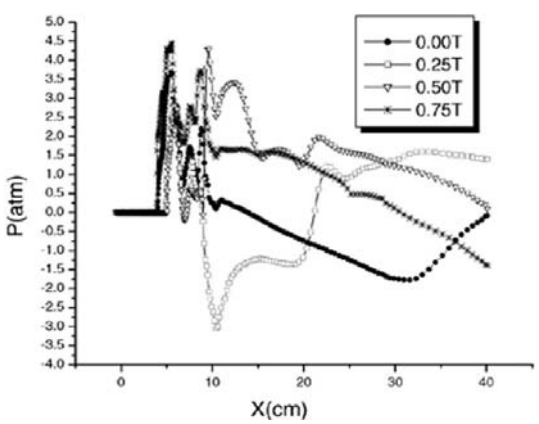

(d) $M=2.5$, $p_b=7.0$ atm, $p_b/p_i=9.459$

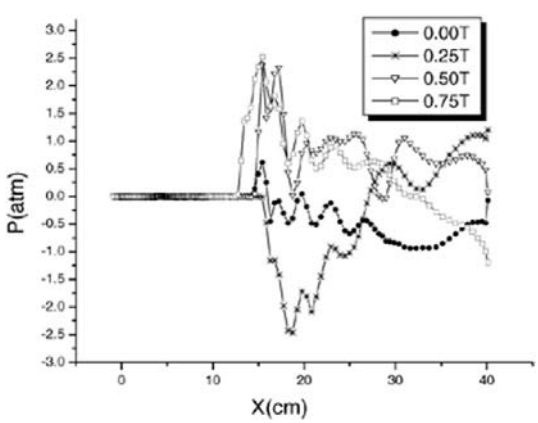

(e) $M=3$, $p_b=6.0$ atm, $p_b/p_i=8.108$

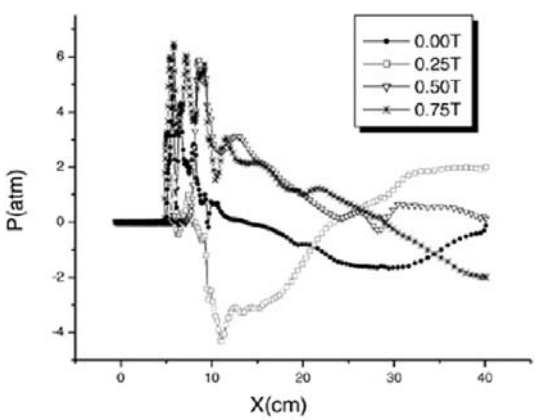

(f) $M=3$, $p_b=10.0$ atm, $p_b/p_i=13.513$

Fig. 8 Pressure difference from the steady state one along the center body at the cruise condition

the normal shock moves downward and the pressure at the neck becomes the lowest, and vice versa. If the pressure is increased to 10 atm at the Mach number 3, the pressure perturbation affects the flow fields in front of the cowl. Figure 7 shows that the normal shock moves back and forth at the front of the cowl. The pressure difference in Fig. 8(f) also shows the same characteristics.

Figure 9 shows the relation between the mass flow rate and perturbed pressure at the cruise condition. The mass flow rate at the Mach number 2 and the exit pressure 4.5 atm, is less than he designed mass flow rate 2.0 kg/s since the normal shock moves in front of the cowl and the flow field is subcritical. Fig. 9(a) shows that there is a regular sudden decrease in the mass flow rate with the downstream pressure perturbation. When the Mach number is 2.5 and the exit pressure is 7 atm, the mass flow rate in Fig. 9(b) shows a regular abrupt decrease whenever the normal shock moves out of the cowl. It shows that the maximum decrease can be 20% of the designed mass flow rate 2.5 kg/s whenever the exit pressure has lower value. When the Mach number is 3.0 and the exit pressure is 10 atm, the mass flow rate in Fig. 9(c) shows the similar behavior but the decrease is small. When the exit pressure is increased to 11 atm at Mach number 3, the normal shock is completely detached from the cowl and the steady state solution is obtained. If the magnitude of the perturbation is 5% instead of 20%,

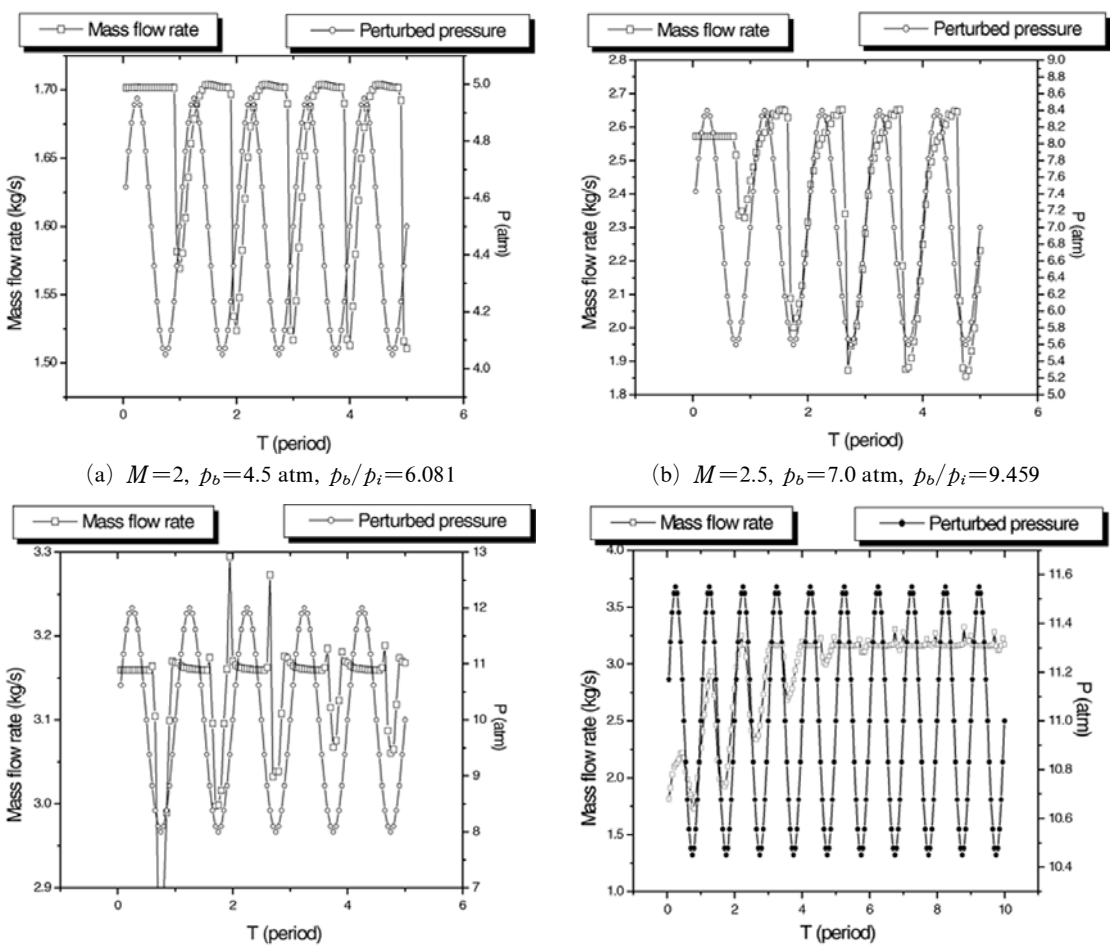

(a) $M=2$, $p_b=4.5$ atm, $p_b/p_i=6.081$ (b) $M=2.5$, $p_b=7.0$ atm, $p_b/p_i=9.459$

(c) $M=3$, $p_b=10.0$ atm, $p_b/p_i=13.513$ (d) $M=3$, $p_b=11.0$ atm, $p_b/p_i=14.865$

Fig. 9 The relation between the mass flow rate and perturbed pressure at the cruise condition

the unsteady solution can be obtained. We found that this small magnitude could change the upstream flow field a lot at this Mach number. Fig. 9(d) shows the relation between the mass flow rate and the perturbed pressure. The unsteadiness is very large in the beginning and becomes weak after the 5 periods.

5. Summary

Flows in a ramjet inlet is simulated for the study of the rocket-ramjet transition. The flow is unsteady, two-dimensional axisymmetric, compressible and turbulent. Double time marching method is used for the unsteady calculation and HLLC method is used as a higher order MUSCL method. As for turbulent calculation, $k-\omega$ SST model is used for more accurate viscous calculations. Sinusoidal pressure perturbation is given at the exit and the flow fields at the inlet is studied. The cruise condition as well as the ground test condition are considered. The pressure level for the ground test condition at the height of 12.8 km is relatively low and the effect of the pressure perturbation at the combustion chamber is small. The normal shock at the cruise condition at the height of 2.5 km is very sensitive to the pressure perturbation and can be easily detached from the cowl when the exit pressure is relatively high. When the shock is detached from the cowl and the inlet flow becomes subcritical, the perturbation at the combustion chamber can change the outside flow. The sudden decrease in the mass flux is observed when the inlet flow becomes subcritical, which can make the inlet incapable. The amplitude of travelling pressure waves becomes larger as the downstream pressure increases, and the wavelength becomes shorter as Mach number increases. The phase difference of the travelling perturbed pressure wave in space is 180 degree.

Acknowledgments

This work was supported by 2003 Hongik University Research Fund.

References

Dailey, C. L., 1955, "Supersonic Diffuser Instability," *Journal of the Aeronautical Sciences*, Vol. 22, No. 11, pp. 733~749.

Kim, S. D., Kwon, C. O. and Song, D. J., 2004, "Comparison of Turbulence Models in Shock-Wave/Boundary-Layer Interaction," *KSME International Journal*, Vol. 18, No. 1. pp. 153~166.

Lu, P. J. and Jain, L. T, 1998, "Numerical Investigation of Inlet Buzz Flow," *Journal of Propulsion and Power*, Vol. 14, No. 1, pp. 90~100.

Menter, F. R., 1994, "Two-equation Eddy-Viscosity Turbulence Models for Engineering Applications," *AIAA Journal*, Vol. 32, No. 8. pp. 1598~1605.

Newsome, R. W., 1984, "Numerical simulation of Near-Critical and Unsteady, Subcritical Inlet Flow," *AIAA Journal*, Vol. 22, No. 10, pp. 1375~1379.

Roe, P. L., 1981, "Approximate Riemann Solvers, Parameter Vectors, and Difference Schemes," *J. Comput. Phys.*, Vol. 43, pp. 357~372.

Shigematsu, J. and Yamamoto, K., 1990, "A Numerical Investigation of Supersonic Inlet Using Implicit TVD Scheme," *AIAA Paper* 90-2135.

Toro, E. F., 1997, "Riemann Solves and Numerical Methods for Fluid Dynamics," Springer.

Wilcox, D. C., 1988, "Reassessment of the Scale-Determining Equation for Advanced Turbulence Model," *AIAA Journal*, Vol. 26, No. 11, pp. 1299~1310.